Electrodissolution and Passivation of Silicon in Aqueous Alkaline Media: A Voltammetric and Impedance Investigation

Sandro Cattarin* and Marco M. Musiani

Istituto di Polarografia ed Elettrochimica Preparativa del C. N. R., Corso Stati Uniti 4, 35100 Padova, Italy

Received: June 2, 1998; In Final Form: December 7, 1998

The behavior of Si electrodes in aqueous alkaline media has been investigated by voltammetric and impedance techniques. The flatband potential has been estimated on the basis of Mott−Schottky plots and photocurrent onset as $E_{FB} = -1.15$ V (SCE) for n-Si and $E_{FB} = -0.45$ V(SCE) for p-Si. A dissolution/passivation mechanism is proposed, assuming: (1) irreversible electrochemical oxidation of H-terminated Si to a monohydroxylated surface species, which may undergo either (2) irreversible electrochemical oxidation to a dihydroxylated species responsible of 2D surface blocking or (3) chemical dissolution as Si(II) regenerating an H-terminated surface; furthermore, (4) the blocking species may be dissolved chemically as Si(IV); (5) a chemical reaction with water generating monohydroxilated Si (and H_2) is also considered. A kinetic model is developed for the case of n-Si, assuming Helmholtz-layer control. The model reproduces the essential experimental features of both $J-E$ curves and impedance diagrams in the active dissolution and passivation regions but is not expected to be realistic in the passive region where 3D surface blocking should be considered.

1. Introduction

The process of silicon corrosion in aqueous alkaline medium is of great technological importance. Orientation-dependent etching allows micromachining of silicon wafers for preparation of electronic devices, optical and analytical systems, sensors, etc.[1,2]

Open circuit corrosion in an alkaline solution is reported to occur with production of two H_2 molecules for each silicon atom,[3] with dissolution of species, such as $SiO_2(OH)_2^{2-}$ and other similar species,[4] probably in a polymeric form. The $J-E$ curve of silicon anodization in alkali is N-shaped, as frequently observed for the dissolution/passivation of metals:[5,6] on sweeping the electrode potential from an open circuit in a positive direction, the current increases up to the passivation peak (PP), then falls to a minimum, and shows passive dissolution on further increases of the applied voltage.[7,8]

The phenomena have been studied with electrochemical[3,7,8] and spectroscopic techniques[3,9] as well as scanning tunneling microscopy (STM) methods.[10,11] The hydrophobic character of both (100) and (111) surfaces at an open circuit and during anodic dissolution at potentials negative of the PP is taken as evidence of H-termination. An increase of OH-termination is assumed on approaching the PP, and passivation is attributed to formation of Si−O−Si bridges at Si sites with two bondings to the crystal.[3,11−14] The thickness of the passivating film is a matter of some controversy. Whereas, Faust et al.[7,12] estimated the oxide thickness at potentials slightly positive to the PP at several monolayers on the basis of ellipsometric data, other authors[10,11] have given evidence of an oxide coverage on the order of one or two monolayers.

Considering the limited literature on impedance of this system,[15] we have investigated the voltammetric and impedance behavior of both p- and n-Si in 2 M NaOH. Results are discussed in terms of a convenient equivalent circuit, comprising passive elements and a faradic impedance that has been calculated for a mechanism involving 2D passivation.

2. Experimental Section

Silicon (100) wafers (thickness 381 ± 25 μm) were purchased from Semimetrics Ltd. Reported experiments were made with n-Si and p-Si materials with similar resistivity (7.5−11 and 8−12 Ω·cm, respectively). Si crystals were back-contacted with an indium−gallium eutectic and fixed with a silver epoxy to brass holders. After final sealing with an epoxy resin (Scotchcast 3M 10/XR 5241), the electrodes had surface areas in the range from 0.20 to 0.28 cm^2.

Solutions were prepared from water deionized by a Millipore Milli-RO system, and analytical grade NaOH (Merck or Carlo Erba) was used without further purification. Experiments were performed in a thermostated glass cell equipped with an optical flat.

In impedance experiments, a working and a counter electrode were inserted in the same compartment, facing each other. In photoelectrochemical experiments, the working electrode was oriented conveniently for illumination (white light from a 150 W Xe lamp), and the counter electrode was placed in a side compartment. A saturated calomel electrode (SCE) inserted in a sidearm and connected to the main compartment by a Luggin capillary was used as a reference, and all potentials were referenced to SCE.

Prior to electrochemical experiments, the electrodes were etched in 2 M NaOH for several minutes until complete removal of the oxide layer, as shown by stabilization of the open circuit potential (at about −1.4 V for n-Si and −1.3 V for p-Si) and H_2 evolution. Operating temperatures from 25 to 70 °C were explored, but reported data refer only to 45 °C. Solutions were purged from oxygen prior to experiments and maintained under a nitrogen stream.

The ac impedance experiments were performed with a Solartron 1254 frequency response analyzer and a Solartron

* To whom correspondence should be addressed.

10.1021/jp982462t CCC: $18.00
Published on Web 04/06/1999

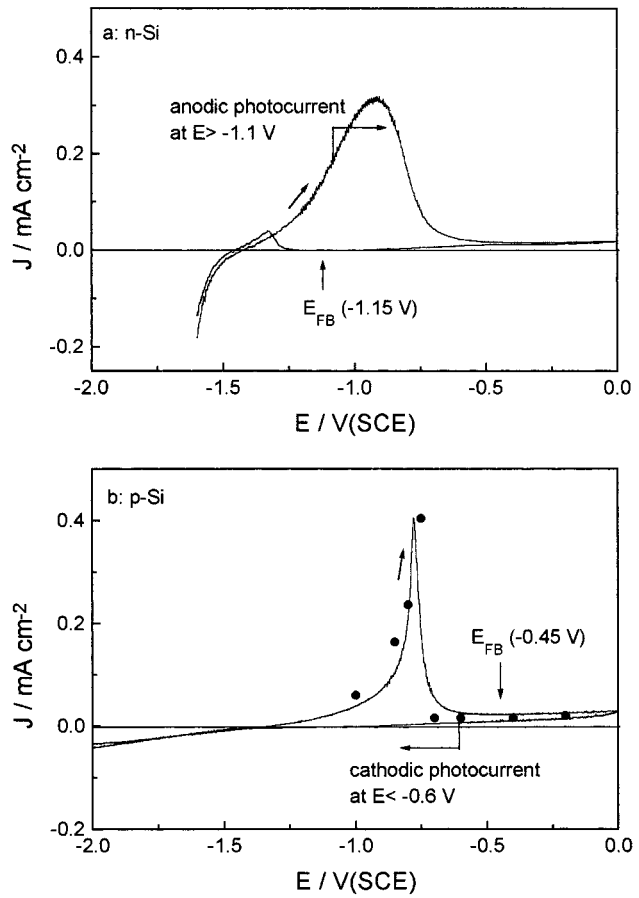

Figure 1. Cyclic voltammograms recorded at 45 °C in 2 M NaOH in the dark. Sweeps were performed from the negative limit to 0.0 V and backward (10 mV s^{-1}) for both silicon types. Potentials of photocurrent onset and estimated flatband potential E_{FB} are indicated. The voltammetric curve is compared in (b) with quasi-stationary current values (dots) observed during impedance measurements.

1286 electrochemical interface, both computer driven by commercial software (FRACOM), which was also used for determining resistance and capacitance values. Impedance plots were obtained under potentiostatic control, generally in the frequency range 10 mHz to 63 kHz (8 points per decade).

3. Results and Discussion

3.1. Voltammetric Investigations. The open circuit potential of n-type and p-type (100) Si in 2.0 M NaOH at 45 °C is about −1.40 and −1.30 V (vs SCE), respectively. The voltammetric patterns are reported in Figure 1. From the negative side of the open circuit, the dominant process is hydrogen evolution, which is the limit of a p-Si because of the lack of electrons. From the positive side of the open circuit, the current turns anodic from the electrode dissolution process. Similar voltammetric profiles are obtained for the two Si types, although the peak shape is different: rather broad and centered around −0.90 V for an n-Si (Figure 1a); sharper and with a steeper passivation (maximum at about −0.75 V) for a p-Si (Figure 1b). The flow of a large anodic current at an n-Si despite its lack of holes may be accounted for by an electron injection process.[13] The same must be true for the oxidation process at a p-Si close to an open circuit, where the material is under strong depletion;[16] hole capture may contribute significantly in the peak region and in the passivation range.

During the backward potential sweep from the positive limit, the current peak is absent for a p-Si (Figure 1b) and small for an n-Si (Figure 1a), indicating surface passivation. The small peak observed for an n-Si indicates that residence at potentials negative to the PP results in reactivation of the dissolution process. The same phenomenon is observed at p-Si electrodes only at slower sweep rates or higher electrolyte temperatures, suggesting growth of a thicker oxide in the passive domain.

Photocurrent/voltage curves have been recorded to get information on the flatband potential. To avoid or, at least, limit the effects of surface oxidation, the Si electrodes were etched in NaOH until hydrogen evolution ceased, and then a potential scan was performed from a convenient negative limit (as in Figure 1). At the n-Si, the onset of anodic photocurrent occurs at −1.10 V vs SCE, about 300 mV positive to an open circuit (Figure 1a), where the surface is still hydrogenated. At the p-Si, the cathodic photocurrent disappears at about −0.6 V, which is beyond the PP (oxidized surface).

3.2. Impedance Investigation. Steady-state conditions appropriate for performing impedance experiments were easily obtained at low dissolution currents and in the passive region. Instead, at E near the peak potential, a significant current variation was observed during the measurements; to keep the drift observed during registration of the whole impedance diagram within a few percent, signal averaging at each frequency was limited at most to 200 s. The average current values measured during the impedance experiments were very close to those obtained in the forward sweep of the cyclic voltammetries, as shown, for instance, in Figure 1b.

Figures 2 and 3 show impedance diagrams obtained on an n-Si and a p-Si, respectively; for each electrode, the different diagrams were obtained at potentials negative (a), slightly positive (b), or positive (c) of the peak potential, i.e., in the active dissolution (a), passivation (b), or passive (c) region. In the case of the n-Si (Figure 2), two loops are evident in each diagram, but the characteristic frequencies of these loops are much different in the corresponding regions: in diagrams a and b, two capacitive loops are detected at medium frequency (mf, characteristic frequency of hundreds of Hz) and low frequency (lf, below 1 Hz), while diagram c shows a loop at high frequency (hf, characteristic frequency in the tens of kHz region) and one at mf (tens of Hz). In the case of p-Si, three loops appear in the active dissolution (Figure 3a) and passivation (3b) regions at hf (tens of kHz), mf (tens or hundreds of Hz), and lf (below 1 Hz), though in Figure 3b, the hf loop is only partially visible. Furthermore, in Figure 3b, an additional poorly resolved feature is found between the mf and lf loops. In the passive region (3c) where impedance increases markedly, a single loop is detected at mf.

For each Si type, the hf loop is detectable only at potentials where the material is expected to be under a significant depletion condition ($E \geq -0.7$ V for n-Si and $E \leq -0.75$ V for p-Si), irrespective of the fact that the system is in the active dissolution, passivation, or passive region. The associated resistance increases markedly by increasing the potential for n-Si and decreasing the potential for p-Si, namely, by moving toward stronger depletion conditions. This behavior and the fact that the capacitance associated with the hf loop generally amounts to tens of nF cm^{-2} suggest that the hf loop may be ascribed to the space-charge region (depletion layer). This attribution is supported by the fact that the loop, observed in the dark at appropriate potentials, disappears under illumination (Figure 4). In the latter conditions, the mf loop is still visible but undergoes a modification in size because of changes in the interfacial kinetics, apparent from variations of the steady-state current, which becomes larger for the n-Si (anodic photocurrent) and

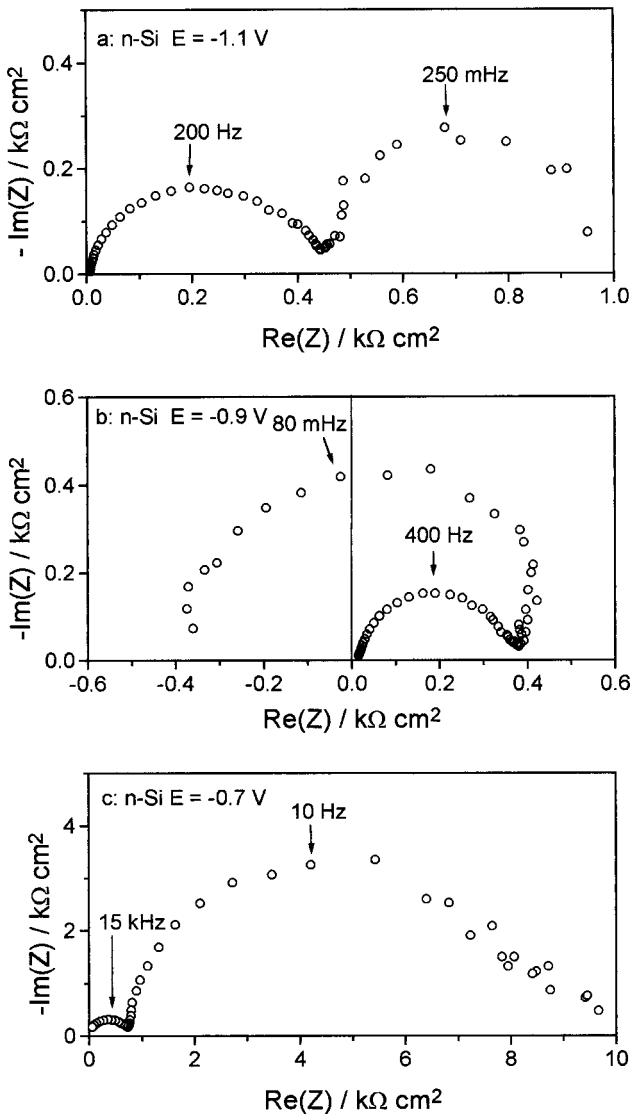

Figure 2. Impedance diagrams for n-Si in 2 M NaOH in the active dissolution (a), passivation (b), and passive dissolution (c) region. The potential is indicated on each figure.

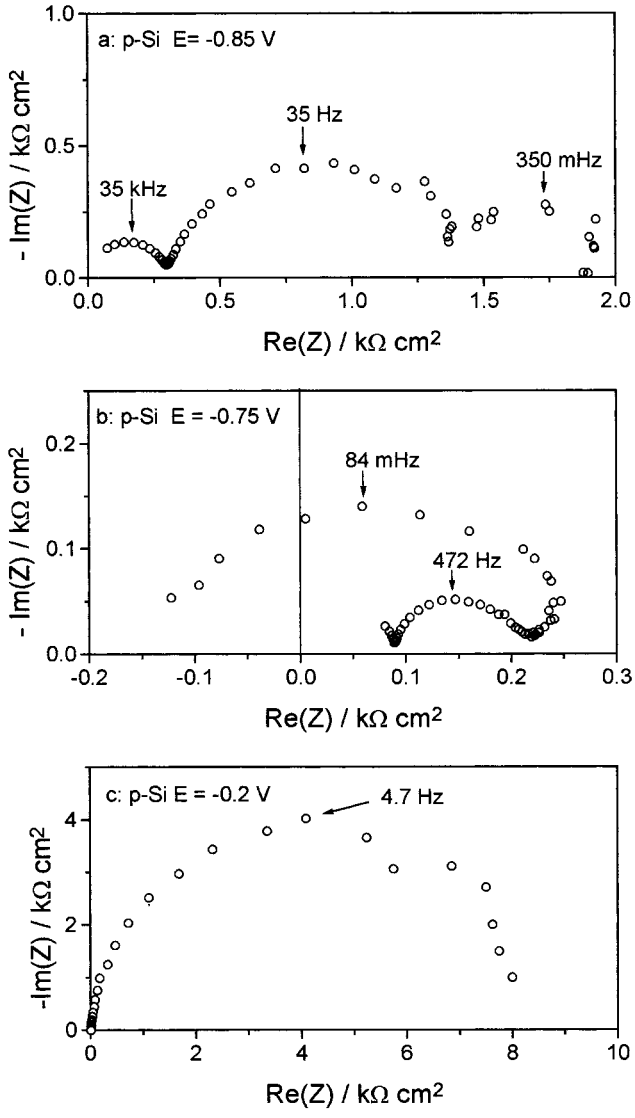

Figure 3. Impedance diagrams for p-Si in 2 M NaOH in the active dissolution (a), passivation (b), and passive dissolution (c) region. The potential is indicated on each figure.

changes from positive to negative for the p-Si (cathodic photocurrent). In the case of n-Si, there is also evidence of a lf loop.

For both Si types, the mf loop is due to the parallel combination of a capacitance of a few μF cm^{-2} with a resistance that goes through a minimum at the peak potential, as shown in Figure 5. The resistance values are similar for n- and p-Si; in the latter case, determination of the mf resistance is prevented at $E > -0.6$ V by the large increase in the size of the hf loop. Both the value of capacitance and the potential dependence of resistance suggest that the mf loop is associated with a double layer (or Helmholtz layer) charging and a charge transfer at the Si−electrolyte interface; for this reason, the relevant resistance has been indicated in Figure 5 as R_t, charge-transfer resistance.

The low-frequency loop in the diagrams of Figures 2 and 3 is due to the parallel combination of a large-pseudo-capacitance (>1 mF cm^{-2}) with a resistance that changes from positive to negative at the peak. These features are common in the impedance diagrams recorded on metals in the passivation region.[17−22] Therefore, the low-frequency loop and the additional feature visible in the medium-to-low frequency domain may be ascribed to relaxation of potential-dependent coverage by surface species, as described below.

According to the above qualitative analysis, the experimental responses will be discussed in comparison with the equivalent circuit of Figure 6, which is similar to circuits suggested by other workers:[23−25] R_{el} represents the uncompensated electrolyte resistance, R_{sc} and C_{sc} are the resistance and capacitance of the space charge region, C_d is the double layer capacitance, and Z_F is the faradic impedance of the dissolution passivation process, which reduces to R_t at sufficiently high frequency. The path marked J_{ph} indicates that under illumination the R_{sc} element is shunted.

3.3. Determination of Flatband. An estimate of flatband position may be obtained from Mott−Schottky plots.[26] For p-Si, a plot of the hf capacitance as C^{-2} vs potential shows an extended linear region in the potential range negative to an open circuit (Figure 7), and a deviation from linearity toward smaller capacitances as the current turns anodic. This observation may originate from a decrease of the active surface, e.g., dissolution of the pyramids formed during chemical etching at negative potentials,[13,14] or from some other interface modification. Extrapolation of the linear portion of the C^{-2} vs E plot intersects the potential axis at −0.45 V (Figure 7). This is a flatband value estimated from measurements performed on an oxide-free surface. Considering that during potential sweeps from the

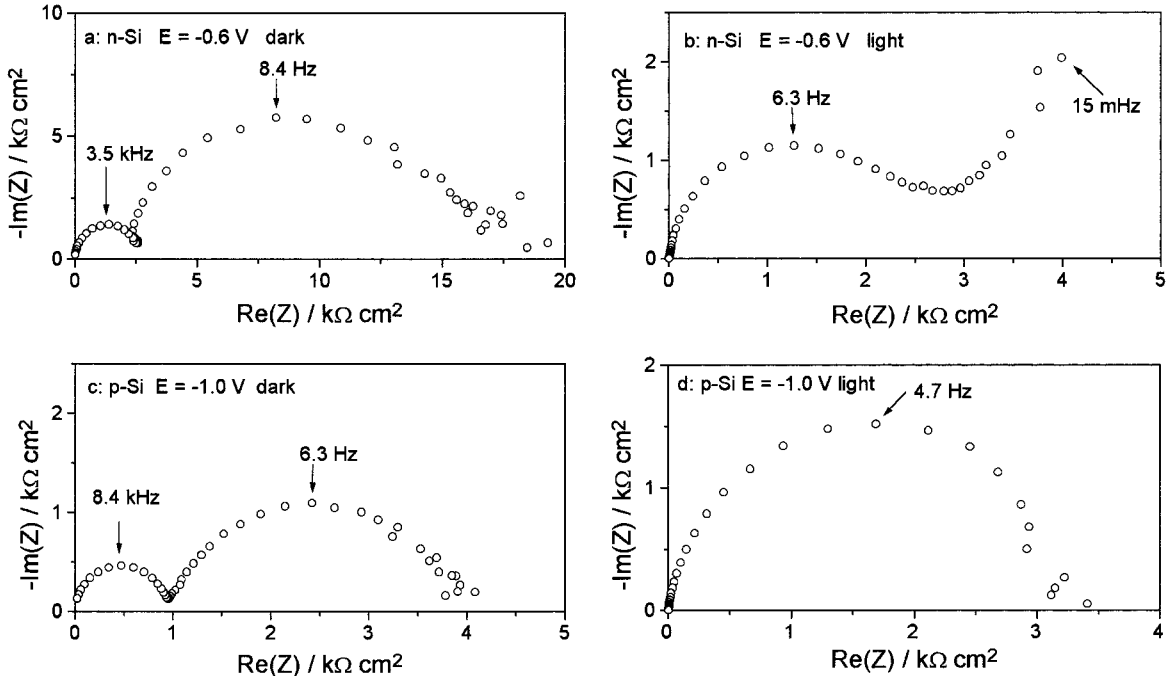

Figure 4. Effect of light on the impedance diagrams of n-Si (a, b) and p-Si (c, d), recorded under depletion conditions, namely, in the passive (n-Si) and active dissolution (p-Si) regions. The potentials are indicated. Illumination was achieved by white light from a xenon lamp.

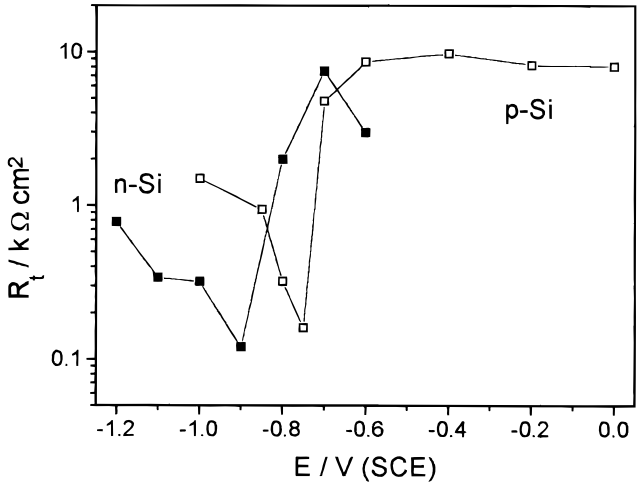

Figure 5. Potential dependence of the medium-frequency resistance, identified as the charge-transfer resistance R_t, measured for either n-Si or p-Si.

negative limit in a positive direction, the cathodic photocurrent disappears around $E_{on} = -0.6$ V, which is beyond the passivation peak, with band shifts associated with surface passivation should be rather small. From the slope of the Mott−Schottky plot, the doping density of p-Si is estimated as $N_D = 2.7 \times 10^{15}$ cm^{-3}, somewhat larger than the value $N_D = 1.5 \times 10^{15}$cm^{-3} obtained from a resistivity $\rho \cong 10\ \Omega$ cm on the basis of tabulated data;[27] the small discrepancy might originate from surface roughness.

Concerning n-Si, capacitance values estimated from the hf loop at $E > -0.7$ V are similar to those used for the Mott−Schottky plots of p-Si, which is in the range expected for space charge capacitance. However, no good linearity was observed in a plot C^{-2} vs potential for n-Si, probably from the presence of the surface oxide affecting interface capacitance. However, the flatband for n-Si may be estimated with reference to that for p-Si, assuming similar band edges for both materials, with a band gap of 1.12 eV[27] and a distance of about 0.20 eV between band edges and a Fermi level,[27] which led to estimate the

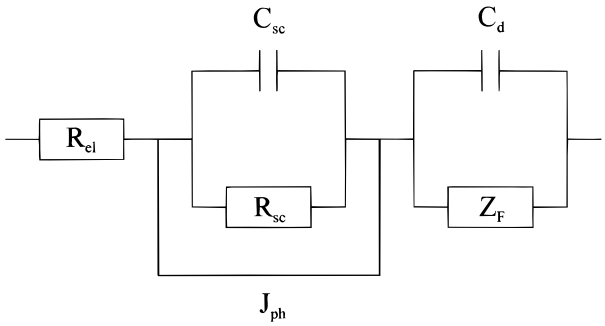

Figure 6. An equivalent circuit adopted for the semiconductor/electrolyte interface: R_{el}, electrolyte resistance; C_{sc} and R_{sc}, capacitance and resistance of the space charge; C_d and Z_F, double layer capacitance and faradic impedance. The effect of light is illustrated by the shunt J_{ph}.

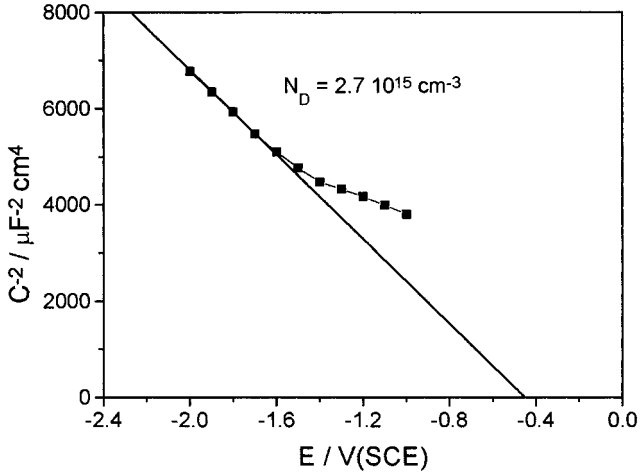

Figure 7. Mott−Schottky plot for p-Si in 2 M NaOH at 45 °C. Flatband potential is estimated as $E_{FB} \cong -0.45$ V.

difference in flatband position between n- and p-Si at about 0.7 eV. Hence, from our data, we can conclude: $E_{FB} = -0.45$ V for p-Si; $E_{FB} = -1.15$ V for n-Si (consistent with photocurrent

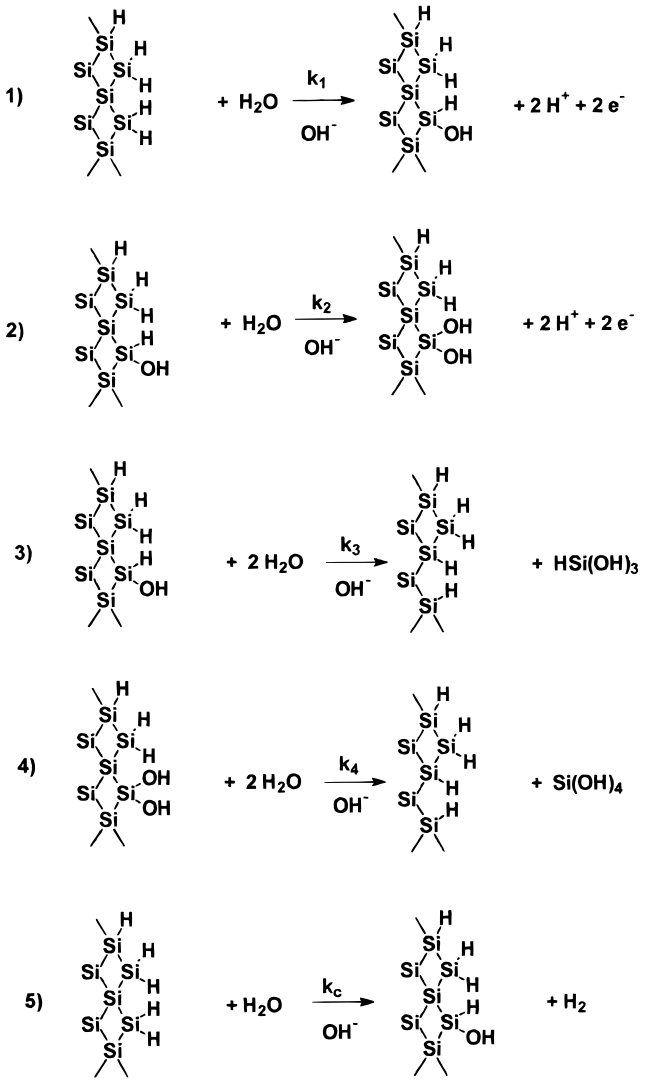

Figure 8. Electrode reactions for the dissolution/passivation processes.

onset). These conclusions, based on evidence from capacitance and photocurrent measurements for both p-Si and n-Si, can be compared with those obtained in a similar medium by Glembocki et al.[8] ($E_{FB} = -1.0$ V for n-Si, $E_{FB} = -0.2$ V for p-Si) based on electroreflectance and capacitance data mentioned but not reported, with those of Allongue et al.[10,11] ($E_{FB} \cong -1.0$ V for n-Si) based on photocurrent onset and with those of Schmuki et al.[28] ($E_{FB} = -1.05$ V for n-Si, $E_{FB} = -0.35$ V for p-Si) obtained in aqueous NH_4OH solutions.

3.4. Dissolution/Passivation: Reaction Scheme and Approximations of the Model. To interpret the observed J−E curves and the faradic impedance, we propose a reaction scheme similar to those discussed in refs 10 and 11, which were represented by the set of five irreversible reactions summarized in Figure 8: (1) electrochemical oxidation (2 e^-) of an hydrogenated $>SiH_2$ species to a $>$SiHOH species; (2) further electrochemical oxidation (2 e^-) of the former $>$SiHOH species to the oxidized $>Si(OH)_2$ species responsible of 2D surface blocking; (3) chemical dissolution of the $>$SiHOH species, producing a Si(II) species that undergoes further oxidation to Si(IV) by chemical reaction with water in solution;[11] (4) chemical dissolution of $>Si(OH)_2$ species directly resulting in dissolved Si(IV); (5) chemical oxidation of $>SiH_2$ to the monohydroxilated $>$SiHOH species. Reaction 5, combined with reaction 3, accounts for the chemical etching of Si that is known to occur in a fairly wide potential range around an open circuit potential. This path does not involve current flow but contributes to the determination of the surface concentration of $>$SiHOH. The electrochemical component of the corrosion process is not considered since it was estimated negligible in comparison with the chemical process.[11] Molecular water is indicated as the main reagent in all reactions while OH^- is considered as a catalyst:[11,13] assuming a [OH^-]-dependent reaction rate would result in a pH-dependent peak height, contrary to observations in this pH range.[11]

Although passivation may involve the formation of Si−O−Si bridges from condensation of neighboring surface Si−OH bonds,[11,13] no other species is explicitly considered since we assume that the behavior of species $>Si(OR)_2$ and $>Si(HOR)$ is the same for R = H or R = Si (neighbor Si atom on the crystal surface). Therefore, the condensation reactions are considered as follow-up processes, affecting neither the current nor the surface fractions θ_1 and θ_2, which represent the coverage in Si atoms bound to one and two oxygen atoms, respectively.

An important point in writing a dissolution mechanism for semiconductors is the potential distribution at the interface and the potential dependence of rate constants. Changes in applied potential may result only (or mainly) in a variation of the band bending (depletion-layer control) or in a change of the potential drop over the Helmholtz layer (Helmholtz-layer control). The two limiting situations have been treated in ref 29 for anodic dissolution of p-Si in HF, considering the impedance of the dissolution process in parallel with the capacitance of the space charge (tens of nF cm^{-2}) or of the Helmholtz layer (μF cm^{-2}), respectively.

In the present paper, we propose a kinetic model for the case of n-Si that allows a simplified treatment. At n-Si, only the process of electron injection is operating because of the lack of holes. In the range from an open circuit to the passivation peak, the semiconductor interface changes from accumulation to mild depletion, and no hf loop corresponding to a depletion layer impedance is observed as it should be if a significant potential drop occurred in the space charge region. Hence, in that potential range, variations of applied potential will be largely (if not entirely) in the Helmholtz layer, and we may assume that electrochemical rate constants will have the form $k = k^0 \exp(\alpha nFE/RT) = k^0 \exp(bE)$, α being the transfer coefficient for the injection process and n the number of electrons. With b treated as a parameter, even a partial Helmholtz control may be accounted. Our only simplification consists of using a constant value for b; complications arising, e.g., from the presence of surface states are neglected.

On the other hand, the anodic reaction at p-Si must involve both electron injection and hole capture. The presence of an hf loop associated with a low capacitance (tens of nF cm^{-2}, Figure 3a,b) shows that a significant potential drop occurs in the depletion layer. However, the strong resemblance of $J-E$ curves, impedance diagrams, and R_f/E curves for the two silicon types (Figures 1−3 and 5), strongly suggests the presence of a partial Helmholtz control even for p-Si (mixed control). Owing to its higher complexity, the case of p-Si will be discussed only qualitatively by comparison with n-Si.

3.5. Dissolution/Passivation: Kinetic Model. The model is based on the reactions of Figure 8. The current density J flowing across the interface (1 cm^2 electrode area) may be written as:

$$J = 2F[(1 - \theta_1 - \theta_2)k_1 + \theta_1 k_2] \qquad (1)$$

in which θ_1 and θ_2 represent the surface fractions of sites $>Si(HOR)$ and $>Si(OR)_2$ (R = H, Si), respectively, and $(1 - \theta_1 - \theta_2)$ is the fraction of "active" surface, covered by the

$>SiH_2$ species and continuously regenerated by reactions 3 and 4. The time variation of θ_1 and θ_2 is given by

$$\beta\frac{d\theta_1}{dt} = (1 - \theta_1 - \theta_2)(k_c + k_1) - \theta_1(k_2 + k_3) \quad (2)$$

$$\beta\frac{d\theta_2}{dt} = \theta_1 k_2 - \theta_2 k_4 \quad (3)$$

where β is a constant, assumed for simplicity equal for the two species, which converts θ to surface concentration. The kinetic constants k_1 and k_2 include a constant surface concentration and are potential dependent: $k_1 = k_1^0 \exp(b_1 E)$; $k_2 = k_2^0 \exp(b_2 E)$. The steady-state values of θ_1 and θ_2, henceforth indicated as $\bar{\theta}_1$ and $\bar{\theta}_2$, may be obtained from eqs 2 and 3

$$\bar{\theta}_1 = \frac{(k_c + k_1)k_4}{A} \quad (4)$$

$$\bar{\theta}_2 = \frac{(k_c + k_1)k_2}{A} \quad (5)$$

$$A = (k_c + k_1)k_2 + (k_c + k_1 + k_2 + k_3)k_4 \quad (6)$$

The steady-state current density $\bar{J}$ is obtained by substitution into eq 1:

$$\bar{J} = 2F\frac{k_4}{A}[(k_c + 2k_1)k_2 + k_1 k_3] \quad (7)$$

The average dissolution rate v_d (Si moles dissolved in the unit time) may be computed as $v_d = \bar{\theta}_1 k_3 + \bar{\theta}_2 k_4$ and the average dissolution valence will be the ratio of current to the dissolution rate

$$\bar{z} = \frac{J}{F v_d} = \frac{2[(k_c + 2k_1)k_2 + k_1 k_3]}{(k_c + k_1)(k_2 + k_3)} \quad (8)$$

To calculate the faradic impedance (i.e., the transfer function between the interfacial potential and the faradic current), a small amplitude sinusoidal modulation of potential E is assumed, inducing a sinusoidal variation of θ_1, θ_2, and J. By differentiating eq 1, we obtain:

$$\delta J = 2F[(1 - \bar{\theta}_1 - \bar{\theta}_2)\delta k_1 - k_1\delta\theta_1 - k_1\delta\theta_2 + \bar{\theta}_1\delta k_2 + k_2\delta\theta_1] \quad (9)$$

with $\delta k_1 = b_1 k_1 \delta E$ and $\delta k_2 = b_2 k_2 \delta E$, so that

$$\delta J = 2F\{[(1 - \bar{\theta}_1 - \bar{\theta}_2)b_1 k_1 + \bar{\theta}_1 b_2 k_2]\delta E + (k_2 - k_1)\delta\theta_1 - k_1\delta\theta_2\} \quad (10)$$

Differentiation of eqs 2 and 3 gives

$$\delta\left(\beta\frac{d\theta_1}{dt}\right) = j\omega\beta\delta\theta_1 = (1 - \bar{\theta}_1 - \bar{\theta}_2)\delta k_1 - (k_c + k_1)\delta\theta_1 - (k_c + k_1)\delta\theta_2 - \bar{\theta}_1\delta k_2 - k_2\delta\theta_1 - k_3\delta\theta_1 \quad (11)$$

$$\delta\left(\beta\frac{d\theta_2}{dt}\right) = j\omega\beta\delta\theta_2 = \bar{\theta}_1\delta k_2 + k_2\delta\theta_1 - k_4\delta\theta_2 \quad (12)$$

where $\omega = 2\pi f$, f is the frequency and $j = \sqrt{-1}$. By solving eqs 11 and 12 for $\delta\theta_1$ and $\delta\theta_2$ we obtain, respectively,

$$\delta\theta_1 = k_4\frac{C}{A}\delta E \quad (13)$$

$$\delta\theta_2 = k_4\frac{B}{A}[b_2(k_c + k_1) + C]\delta E \quad (14)$$

where A is given by eq 6 and

$$B = \frac{k_2}{j\omega\beta + k_4} \quad (15)$$

$$C = \{(k_2 + k_3)k_4 b_1 k_1 - (k_c + k_1)(k_c + k_1 + k_4)b_2 k_2 + j\omega\beta[(k_2 + k_3)b_1 k_1 - (k_c + k_1)b_2 k_2]\}/\{(k_c + k_1)k_2 + (k_c + k_1 + k_2 + k_3)k_4 - \omega^2\beta^2 + j\omega\beta(k_c + k_1 + k_2 + k_3 + k_4)\} \quad (16)$$

Inserting now into eq 9 the expressions for $\bar{\theta}_1$, $\bar{\theta}_2$, $\delta\theta_1$, and $\delta\theta_2$ we obtain the faradic impedance $Z_F = \delta E/\delta J$

$$\frac{1}{Z_F} = 2F\frac{k_4}{A}[b_1 k_1(k_2 + k_3) + b_2 k_2(k_c + k_1)] + 2F\frac{k_4}{A}[(k_2 - k_1 - k_1 B)C - b_2 k_1(k_c + k_1)B] \quad (17)$$

The reciprocal of the first term on the right-hand member of eq 17 is the high-frequency limit of Z_F, namely, the charge-transfer resistance R_t.

3.6. Calculated Curves: Comparison with Experiments. To test the model, both steady-state and impedance curves were calculated for a set of kinetic parameters (k_1^0, k_2^0, k_3, k_4, k_c, b_1, and b_2). The model strictly applies to n-Si; however, because of the strong experimental similarity, some comments refer also to p-Si data. Figure 9a shows the $J-E$ curve calculated according to eq 7, Figure 9b shows the potential dependence of $\bar{\theta}_1$ and $\bar{\theta}_2$ (eqs 4 and 5, respectively), Figure 9c shows the R_t-E curve (eq 17), and Figure 9d shows the potential dependence of the dissolution valence $\bar{z}$ (eq 8).

Although no attempt of curve fitting was made, the model reproduces, on the basis of a suitable set of constants, the essential features of our experiments. An asymmetric peak of approximately the right size (Figure 9a) is visible in the calculated $J-E$ curves: J increases as long as $\bar{\theta}_2$ is small and drops when $\bar{\theta}_2$ approaches 1. The values attributed to b_1 and b_2 determine how broad the current peak is; the peak asimmetry in Figure 9a is due to assuming $b_1 < b_2$. At large E, the calculated J becomes constant ($=4Fk_4$), as in the experiments. However, owing to the assumption of 2D surface passivation, the model is not expected to be realistic in the passive region where formation of a thick oxide layer has been reported and ionic transport should be considered.[30] It must be noted that k_4 cannot be zero, as J would be zero at all E values. The values of k_c and k_3 were chosen so as to obtain a chemical dissolution rate at an open circuit in the right range[11] and to keep at the same time $\bar{\theta}_1 \ll 1$, as required by the experimental observation that the surface is mostly hydrogen terminated.[9] Indeed, the value $\bar{\theta}_1 \cong 0.2$ reported in Figure 9b in the negative potential limit corresponds to a coverage in hydroxyl groups around 10%. Assuming $k_c = 0$, i.e., neglecting reaction 5, results in a limit value $\bar{\theta}_1 = 0$ well negative to the peak but does not affect significantly $J-E$ and R_t-E curves reported in Figure 9.

The calculated R_t-E curve (Figure 9c) shows a minimum in the potential range of the current peak, as observed in the experimental data of Figure 5. The dissolution valence changes

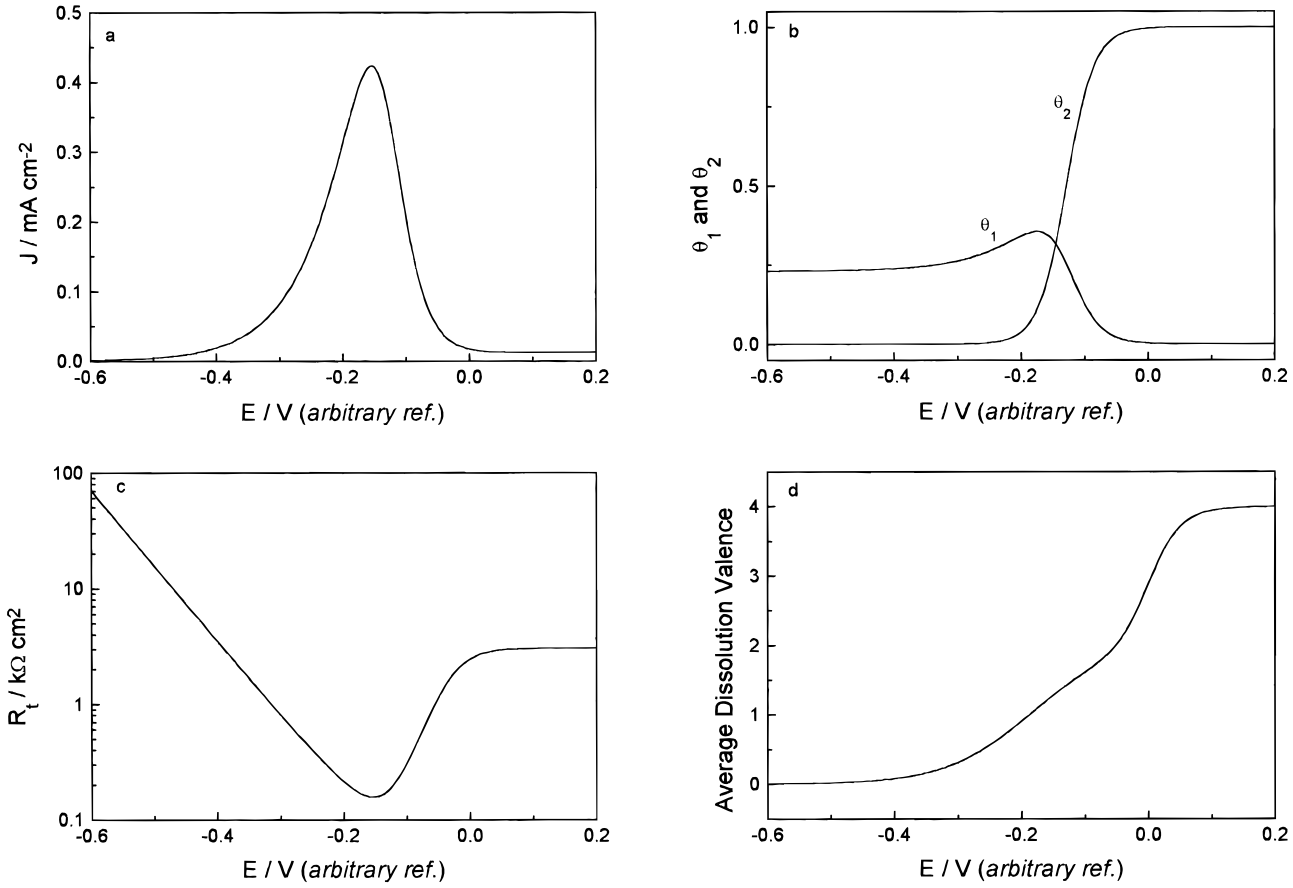

Figure 9. (a) $J-E$ curve for Si dissolution/passivation calculated according to eq 7: $k_1^0 = 5 \times 10^{-8}$ mol cm^{-2} s^{-1}; $k_2^0 = 10^{-8}$ mol cm^{-2} s^{-1}; $k_3 = 10^{-8}$ mol cm^{-2} s^{-1}; $k_4 = 3 \times 10^{-11}$ mol cm^{-2} s^{-1}; $k_c = 3 \times 10^{-9}$ mol cm^{-2} s^{-1}; $b_1 = 15$ V^{-1}; $b_2 = 40$ V^{-1}; (b) Potential dependence of $\bar{\theta}_1$ and $\bar{\theta}_2$ calculated according to eqs 4 and 5 for the same kinetic parameters; (c) Potential dependence of R_t calculated from eq 17 for the same kinetic parameters; (d) Potential dependence of the average dissolution valence $\bar{z}$ calculated from eq 8.

progressively with potential (Figure 9d) from 0 in the active region, where H-termination persists, to a value between 0.5 and 1 at the peak, in agreement with literature observations,[3] and to 4 in the passive region.

Figure 10 shows Nyquist plots of the impedance Z given by

$$\frac{1}{Z} = \frac{1}{Z_F} + j\omega C_d \tag{18}$$

The faradic impedance is, thus, assumed to be in parallel with a double layer capacitance C_d, while any series resistance is neglected. No parallel RC element in series, representing space charge resistance and capacitance (which would produce an additional hf loop) is included. Thus, the calculated plots may show up to three loops, one due to the R_t-C_d combination and two caused by the indirect effect of E on J through the modulation of the surface coverages θ_1 and θ_2.

The impedance plots in Figure 10 are calculated for the same set of kinetic parameters as for Figure 9 and two E values corresponding to the active (a) and passivation (b) region, respectively. Figure 10a shows, from hf to lf, a loop from the R_t-C_d combination, a loop from the modulation of θ_1, and a portion of a loop from the modulation of θ_2. Since the last feature occurs at frequencies falling below the lower experimental limit, Figure 10a reproduces the experimental plots of Figures 2a and 3a well enough, although neither the loop size nor the characteristic frequencies are quantitatively matched. Figure 10b shows, from hf to lf, a loop from the R_t-C_d combination, a region where both real and imaginary part increase and a loop characterized by a negative resistance; the

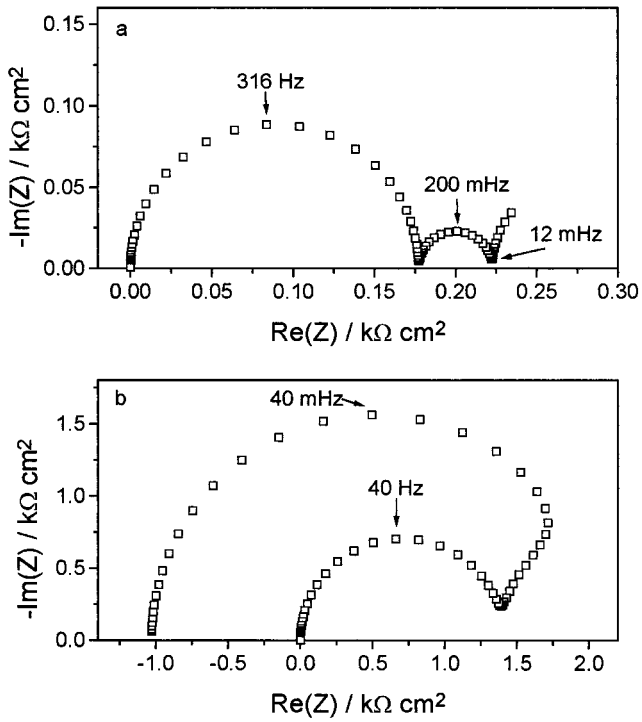

Figure 10. Impedance diagrams for Si dissolution/passivation calculated according to eq 18 with: $k_1^0 = 5 \times 10^{-8}$ mol cm^{-2} s^{-1}; $k_2^0 = 10^{-8}$ mol cm^{-2} s^{-1}; $k_3 = 10^{-8}$ mol cm^{-2} s^{-1}; $k_4 = 3 \times 10^{-11}$ mol cm^{-2} s^{-1}; $k_c = 3 \times 10^{-9}$ mol cm^{-2} s^{-1}; $b_1 = 15$ V^{-1}; $b_2 = 40$ V^{-1}; $C_d = 3 \times 10^{-6}$ F cm^{-2}; $\beta = 10^{-8}$ mol cm^{-2}; $E = -0.18$ V (a) or -0.04 V (b).

last two features, not completely resolved, are associated with modulation of θ_1 and θ_2, respectively. Figure 10b is similar to the experimental diagrams of Figures 2b and 3b, the feature from θ_1 being more clearly visible in the latter than in the former.

Hence, despite some simplifications, the proposed treatment may account for the main experimental observations. A more detailed model, considering additional surface species (and fractions θ_i) or the complications arising from the presence of surface states, is expected to produce impedance diagrams more complex than those actually observed in experiments.

4. Conclusions

The electrodissolution/passivation of Si in 2 M NaOH has been investigated with electrochemical (voltammetry and impedance) and photoelectrochemical methods. The experimental data have been analyzed by an approach combining the use of an equivalent circuit and kinetic modeling. In particular, the hf features of the impedance diagrams have been identified with circuit elements ascribed to space charge region, while a dissolution/passivation mechanism (based on chemical and electrochemical reactions similar to those proposed by previous authors[10−14]) has been developed that satisfactorily accounts for the $J-E$ curves and the mf and lf impedance features.

The proposed model, assuming a Helmholtz layer control of interface kinetics, should apply to n-Si only. However, it seems unlikely that the very similar impedance patterns observed at p-Si (apart from the hf loop) may originate from an entirely different (depletion layer) control: a mixed control may operate in the latter case. The proposed mechanism assumes a passivation caused by 2D surface blocking and is expected to be reliable in the active and passivation regions. At more positive bias, where a "thick" oxide has been detected,[7,12] a realistic model must consider mass transport through the passive layer.[30]

References and Notes

(1) Zavracky, P. M.; Earles, T.; Pokrovskiy, N. L.; Green, J. A.; Burns, B. E. *J. Electrochem. Soc.* **1994**, *141*, 3182.

(2) Kovacs, G. T. A.; Petersen, K.; Albin, M. *Anal. Chem.* **1996**, *68*, 407A.

(3) Palik, E. D.; Glembocki, O. J.; Heard, I. Jr. *J. Electrochem. Soc.* **1987**, *134*, 404.

(4) Palik, E. D.; Gray, H. F.; Klein, P. B. *J. Electrochem. Soc.* **1983**, *130*, 956.

(5) Bockris, J. O'M.; Reddy, A. K. N. In *Modern Electrochemistry*; Plenum Press: New York, 1970.

(6) Pourbaix, M. In *Lectures on Electrochemical Corrosion*; Plenum Press: New York, 1970.

(7) Faust, J. W. Jr.; Palik, E. D. *J. Electrochem. Soc.* **1983**, *130*, 1413.

(8) Glembocki, O. J.; Stahlbush, R. E.; Tomkiewicz, M. *J. Electrochem. Soc.* **1985**, *132*, 145.

(9) Rappich, J.; Lewerenz, H. J.; Gerischer, H. *J. Electrochem. Soc.* **1993**, *140*, L187.

(10) Allongue, P.; Costa-Kieling, V.; Gerischer, H. *J. Electrochem. Soc.* **1993**, *140*, 1009.

(11) Allongue, P.; Costa-Kieling, V.; Gerischer, H. *J. Electrochem. Soc.* **1993**, *140*, 1018.

(12) Palik, E. D.; Faust, J. W. Jr.; Gray, H. F.; Greene, R. F. *J. Electrochem. Soc.* **1982**, *129*, 2051.

(13) Bressers, P. M. M. C.; Pagano, S. A. S. P.; Kelly, J. J. *J. Electroanal. Chem.* **1995**, *391*, 159.

(14) Bressers, P. M. M. C.; Kelly, J. J.; Gardeniers, J. G. E.; Elwenspoek, M. *J. Electrochem. Soc.* **1996**, *143*, 1744.

(15) Abbott, A. P.; Schiffrin, D. J.; Campbell, S. A. *J. Electroanal. Chem.* **1992**, *328*, 355.

(16) Cattarin, S.; Peter, L. M.; Riley, D. J. *J. Phys. Chem. B* **1997**, *101*, 4071.

(17) Armstrong, R. D.; Firman, R. E. *J. Electroanal. Chem.* **1972**, *34*, 391.

(18) Epelboin, I.; Gabrielli, C.; Keddam, M.; Takenouti, H. *Electrochim. Acta* **1975**, *20*, 913.

(19) Epelboin, I.; Keddam, M.; Mattos, O. R.; Takenouti, H. *Corros. Sci.* **1979**, *19*, 1105.

(20) Epelboin, I.; Gabrielli, C.; Keddam, M.; Takenouti, H. In *Comprehensive Treatise of Electrochemistry*; Bockris, J. O'M., Conway, B. E., Yaeger, E., White, R. E., Eds.; Plenum Press: New York, 1981; Vol. 4, p 151.

(21) Macdonald, D. D. *Electrochim. Acta* **1990**, *35*, 1509.

(22) Dobbelaar, J. A. L.; de Wit, J. H. W. *J. Electrochem. Soc.* **1992**, *139*, 716.

(23) Morrison, S. R. In *Electrochemistry at Semiconductors and Oxidized Metal Electrodes*; Plenum Press: New York, 1980.

(24) Chazalviel, J.-N. *J. Electrochem. Soc.* **1982**, *129*, 963.

(25) Schefold, J.; Kühne, H.-M. *J. Electroanal. Chem.* **1991**, *300*, 211.

(26) Gerischer, H. In *Physical Chemistry*, Vol. IXA; Eyring, H., Henderson, D., Jost, W., Eds.; Academic Press: New York, 1970; Chapter 5.

(27) Sze, S. M. In *Physics of Semiconductor Devices*; J. Wiley and Sons: New York, 1981.

(28) Schmuki, P.; Bohni, H.; Bardwell, J. A. *J. Electrochem. Soc.* **1995**, *142*, 1705.

(29) Vanmaekelbergh, D.; Searson, P. C. *J. Electrochem. Soc.* **1994**, *141*, 697.

(30) Ghowsi, K.; Gale, R. J. *J. Electrochem. Soc.* **1989**, *136*, 867.